



# Dual-Band and Dual Polarized Inverted Pentagonal Shaped Hybrid Cylindrical Dielectric Resonator Antenna for Wireless Applications

Chandravilash Rai<sup>1</sup> · Amit Singh<sup>1</sup> · Sanjai Singh<sup>1</sup> · Ashutosh Kumar Singh<sup>1</sup> · Ramesh Kumar Verma<sup>2</sup>

Accepted: 21 November 2021 / Published online: 3 January 2022

© The Author(s), under exclusive licence to Springer Science+Business Media, LLC, part of Springer Nature 2021

## Abstract

This article presents a dual-band dual-polarized, slotted cylindrical dielectric resonator antenna (CDRA) for wireless applications. Multiple inverted pentagons with slotted aperture are used to radiate hybrid mode  $HEM_{11\delta}$ . The suggested radiator has two operating frequency bands: lower frequency band is from 3.75 to 3.96 GHz with 5.44% (210 MHz) fractional bandwidth resonating at 3.87 GHz while upper frequency band is from 6.58 to 8.4 GHz with 24.29% (1820 MHz) fractional bandwidth resonating at 6.63 GHz. The lower resonating band is generated because of multiple slots while upper resonating band is due to the combination of CDRA and multiple slots. The lower band is linearly polarized whereas the upper band is dual-polarized (linear/circular). Circular polarization (CP) characteristic is achieved at the upper frequency band by combining the effect of moon-type microstrip line and multiple slots. Axial ratio bandwidth (3-dB) is obtained about 7.06% (550 MHz) between 7.52 and 8.07 GHz with 0.62 dB minimum AR value at frequency 8.01 GHz. This radiator can be used in partially S and C-band applications.

**Keywords** Cylindrical dielectric resonator antenna (CDRA) · Circular polarization · Microstrip line · Multiple slots · Axial ratio

---

✉ Chandravilash Rai  
cvrai87@gmail.com

Amit Singh  
rse2018504@iiita.ac.in

Sanjai Singh  
ssingh@iiita.ac.in

Ashutosh Kumar Singh  
ashutosh\_singh@iiita.ac.in

Ramesh Kumar Verma  
ramesh85.ec@gmail.com

<sup>1</sup> Department of Electronics and Communication Engineering, Indian Institute of Information Technology Allahabad, Prayagraj, UP, India

<sup>2</sup> Department of Electronics and Communication Engineering, Bundelkhand Institute of Engineering and Technology, Jhansi, UP, India

## 1 Introduction

Dielectric resonator antenna (DRA) is one of the popular antennas during the last three decades because of its essential characteristics such as large impedance bandwidth, substantial gain, smaller in size, high radiation efficiency (no conduction losses) and economical [1, 2]. DRA is available in different shapes like rectangular, cylindrical, hemispherical, or any other shape. But cylindrical and rectangular DRA is more useful because of their design flexibility and economical availability [1]. The cylindrical dielectric resonator antenna (CDRA) has three ( $TE_{mnp}$ ,  $TM_{mnp}$  and  $HE_{mnp}$ ) modes, each of them are useful for obtaining a particular radiation pattern [3].

Dual/multi-band DRA is more useful in wireless communication because a single antenna can be used in more than one application. Mainly three techniques is used to achieve dual/multi-band characteristics: (1) Hybrid DRA [4, 5], (2) Using parasitic element with DRA [6] and (3) Creating higher order modes in addition to the basic mode of DRA [7]. Out of three, the last one is more fruitful, however it is quite complicated to develop a higher order mode in DRA [8, 9].

In today's world of wireless communication, researchers are concentrating their efforts on dual-polarized antennas, which are unaffected by propagation direction and obey multipath between the transmitter and receiver [10]. In single feed DRA, there are many methods for obtaining circular polarization (CP) in DRA using distinctive geometry like elliptic DRA showing 3.5% AR bandwidth along with 14% impedance bandwidth [11], Super shape DRA (S-DRA) [12], Trapezoidal DRA [13], stacked CDRA with half split [14] and stacked rectangular DRA [15] using different permittivity. DRA excitation using cross slot with 3.91% (80 MHz) AR bandwidth [16], DRA of large size 75 mm×75 mm with CP using slotted ground [17] showing AR bandwidth of 2.7% (59 MHz) and DRA excited with helical shape exciter [18] exhibiting 6.4% AR bandwidth along with 10.2% impedance bandwidth, microstrip line feed of question mark shape cubic DRA [19] and rectangular DRA with partial ground using meandered line [20], ring DRA of size 50 mm×45 mm with polygon of hexagonal shape [21], four ports MIMO antenna of large size 80 mm×80 mm providing 20.86% (750 MHz) and 10.71% (560 MHz) impedance bandwidth [22] and CDRA with T-shape line feed having slot of square ring shape [23] is also presented. Some other dual band antennas based on DRA with CP characteristic is designed using triangular shape aperture [24] of size 40 mm×40 mm, omnidirectional CDRA [25] with 5.71% and 7.99% impedance bandwidth, omnidirectional CDRA of radius 30 mm having CP with circular patch [26], rectangular DRA of very large size 100 mm×100 mm showing impedance bandwidth of 11.4% and 8.4% using cross slot [27], CDRA of size 40 mm×40 mm with swastik shape aperture [28], eccentric semi annular elliptical DRA [29] exhibiting CP with 5.71% AR bandwidth, omnidirectional rectangular DRA excited with coaxial probe having 4.57% (210 MHz) AR bandwidth [30], V-shape microstrip line based CDRA of size 50 mm×50 mm using modified slot [31] and ring shape DRA of size 50 mm×50 mm with T-shape line feed having circular ring [32].

In the proposed work, a dual band characteristic is generated using multiple inverted pentagon slots and CDRA. The lower operating frequency band from 3.75 to 3.96 GHz is created due to multiple inverted pentagon slots and the upper operating band from 6.58 to 8.4 GHz is generated because of the combining effect of CDRA and multiple slots. An orthogonal field is created due to the moon-like microstrip line and multiple inverted pentagon slots. Because of this field, circular polarization (CP) achieves at the upper frequency band from 7.52 to 8.07 GHz with axial ratio (3-dB) bandwidth of 7.06% whereas the lower

band is only linearly polarized. The lower frequency band from 3.75 to 3.96 GHz provides the services in S-band whereas the upper frequency band from 6.58 to 8.4 GHz comes under the category of extended C-band application and useful for the earth to space communication [33].

The content of proposed work is organized in following sections. The proposed CDRA geometry and step by step design with parametric analysis are presented in Sect. 2 and Sect. 3 respectively. The results discussion along with experimental outcomes and performances comparison with pervious work are discussed in Sect. 4. Finally, overall conclusion of proposed work is described in Sect. 5.

## 2 Antenna Geometry

The diagram of the proposed radiator is shows in Fig. 1a–c. It is built on a marginal price FR4 substrate ( $\epsilon_r, \text{sub}=4.4$ ,  $\tan\delta=0.02$  and  $h=1.6$  mm) with width  $W_S=40$  mm and length  $L_G=40$  mm. Multiple inverted pentagon shapes are slotted on the ground plane

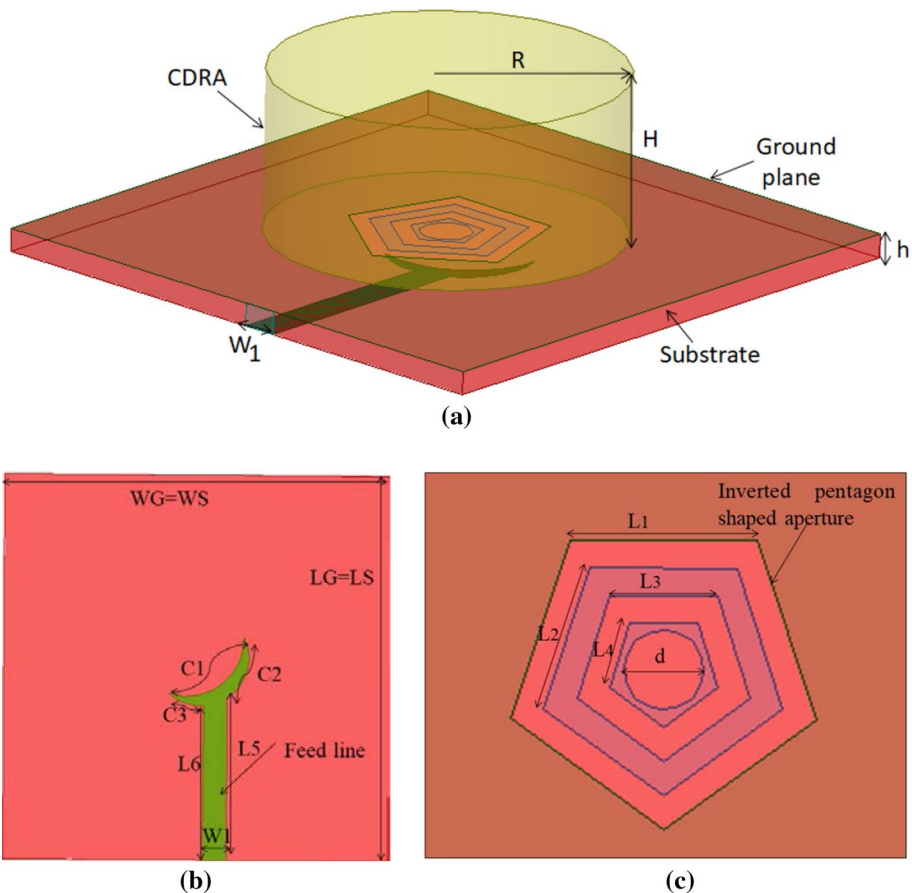


**Fig. 1** Schematic diagram **a** perspective view, **b** feeding structure, **c** top view without CDRA feed line

of the substrate. A half moon shaped microstrip line (50Ω) is placed below the substrate. A cylindrical dielectric resonator (Alumina:  $\epsilon_r$  CDRA=9.8 and  $\tan\delta=0.002$ ) of height  $H=11.1$  mm and radius  $R=12$  mm is placed above the substrate. Details optimized dimensions are given in Table 1.

The resonant frequency of hybrid mode HEM<sub>11δ</sub> with CDRA is computed by [10].

$$f_r, HEM_{11\delta} = \frac{6.321c}{2\pi R\sqrt{\epsilon_{r,eff} + 2}} \left[ 0.27 + 0.36\left(\frac{R}{2H_{eff}}\right) + 0.02\left(\frac{R}{2H_{eff}}\right)^2 \right] \tag{1}$$

where  $H_{eff}$  and  $\epsilon_{reff}$  are the effective height and permittivity while  $R$  is radius of CDRA.  $H_{eff}$  and  $\epsilon_{reff}$  are calculated by following formulas [1].

$$\epsilon_{r,eff} = \frac{H_{rff}}{\frac{H}{\epsilon_{r,CDRA}} + \frac{H_s}{\epsilon_{r,Sub}}} \tag{2}$$

$$H_{eff} = H + H_s \tag{3}$$

By using these equations, the theoretical value for HEM<sub>11δ</sub> mode is identified to be 3.87 GHz.

### 3 Parametric Analysis

The effect of various parameters on the performance of the proposed CDRA are discussed in this section. The Ansys HFSS simulator is used to analyzed and optimized the antenna design. The parametric analysis is divided into two parts: (1) Reflection coefficient ( $S_{11}$ ) and (2) Circular polarization (CP) characteristics.

#### 3.1 Reflection Coefficient ( $S_{11}$ )

Step to step design procedure of the proposed CDRA is presented in Fig. 2 and its corresponding reflection coefficient vs frequency graph is shown in Fig. 3. In step 1, step 2 and step 3, the antennas are excited with single, double and triple inverted pentagon shape slot aperture using simple microstrip feed line whereas the antenna designed in

**Table 1** Optimized parameter of the proposed CDRA

Symbol	Dimension (mm)	Symbol	Dimension (mm)
LG=LS	40	C3	3.91
WG=WS	40	L1	8.22
H	11.1	L2	6.46
R	12	L3	4.70
h	1.6	L4	2.93
W1	2.43	L5	16.81
C1	10.15	L6	16
C2	7.22	d	3.48

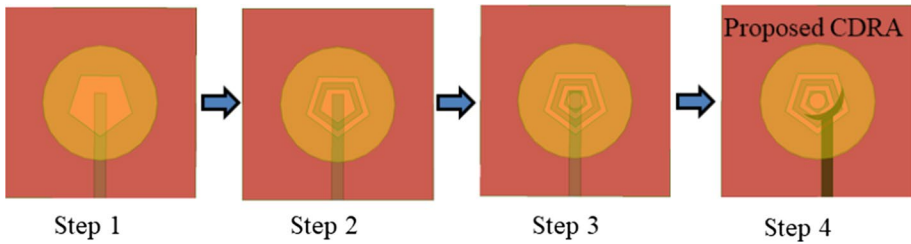


Fig. 2 Stepwise design procedure of proposed CDRA

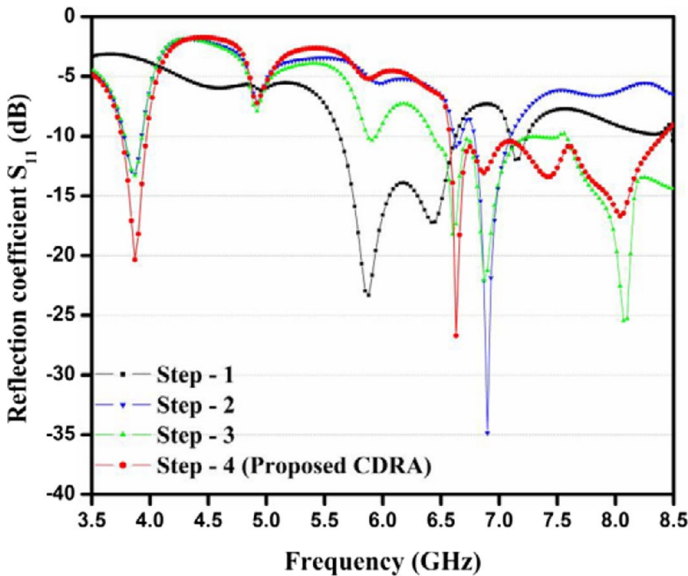


Fig. 3 Reflection coefficient versus frequency graph with step to step design procedure

step 4 with circle on the place of third inverted pentagon shape slot aperture using half-moon type microstrip feed line. The antennas designed in step 1, step 2 and step 4 are resonating in dual band while antenna designed in step 3 is resonating in multiple band. The fractional bandwidth of proposed CDRA in step 4 compared to step 3 is improved due to circle in place of third pentagon slot and half-moon type microstrip feed line. The fractional bandwidth of 16.31% (1000 MHz) and 2.09% (150 MHz) resonating at 5.88 GHz and 7.14 GHz in step 1 while 4.42% (170 MHz) and 4.32% (300 MHz) resonating at 3.87 GHz and 6.9 GHz in step 2 is obtained. The antenna designed in step 3 using triple inverted pentagon slot is resonating in multiband at frequencies 3.78 GHz, 6.87 GHz and 8.07 GHz with poor reflection coefficient and narrow bandwidths. While antenna designed in step 4 is resonating in dual band with fractional bandwidth of 5.44% (210 MHz) in lower band between 3.75 and 3.96 GHz at frequency 3.87 GHz and 24.29% (1820 MHz) in upper band between 6.58 and 8.40 GHz at frequency 6.63 GHz.

### 3.1.1 Effect of CDRA

Figure 4 displays the reflection coefficient vs frequency graph of antenna without and with CDRA. It is confirmed from Fig. 4 that the lower operating frequency band is due to CDRA and the upper operating frequency band is because of the combined effect of with and without CDRA. Thus the proposed CDRA is considered as a hybrid antenna. The antenna without CDRA is resonating in single band from 6.03 to 7.86 GHz with fractional bandwidth of 26.34% (1830 MHz) at frequency 7.14 GHz while antenna with CDRA is resonating in dual band from 3.75 to 3.96 GHz with fractional bandwidth of 5.44% (210 MHz) in lower operating band at frequency 3.87 GHz while 6.58 GHz to 8.4 GHz with fractional bandwidth of 24.29% (1820 MHz) in upper operating band at frequency 6.63 GHz.

### 3.1.2 Effect of Height (H) and Radius (R) of CDRA

To optimized the antenna, the height (H) and radius (R) of CDRA are varied in step of 0.5 mm and its effect on the reflection coefficient is observed as shown in Figs. 5 and 6 respectively. In the observation of parametric variation, one parameter is varied while other is kept constant. The effect of height (H) variation on the reflection coefficient is observed at H=10.1 mm, 10.6 mm, 11.1 mm, 11.6 mm and 12.1 mm as shown in Fig. 5 while the effect of radius (R) variation on the reflection coefficient is observed at R=11 mm, 11.5 mm, 12 mm, 12.5 mm and 13 mm as shown in Fig. 6. In variation of height (H), the antenna is resonating in dual band with fractional bandwidth of 5.44% (210 MHz) and 24.29% (1820 MHz) for H=11.1 mm and 5.49% (210 MHz) and 24.19% (1800 MHz) for H=11.6 mm while antenna is resonating in multiband at frequencies 3.96 GHz, 6.72 GHz and 7.59 GHz for H=10.1 mm, 3.93 GHz, 6.69 GHz and 8.72 GHz for H=10.6 mm and 3.81 GHz, 6.57 GHz and 8.04 GHz for H=12.1 mm.

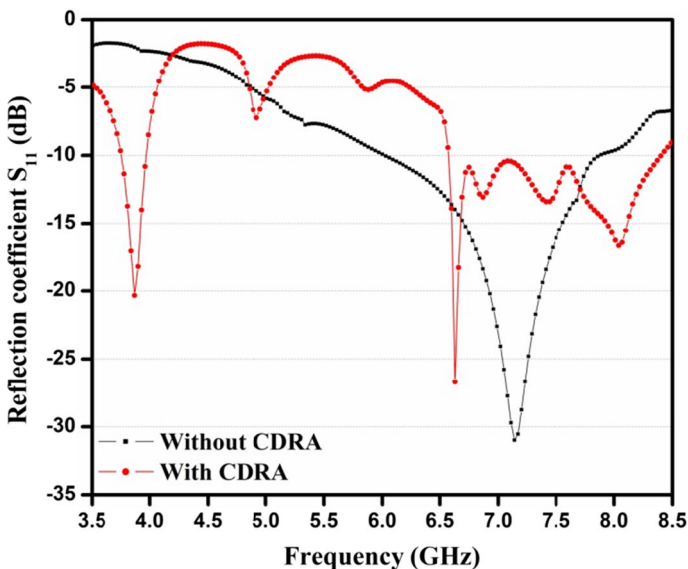


Fig. 4 Reflection coefficient versus frequency graph with and without CDRA

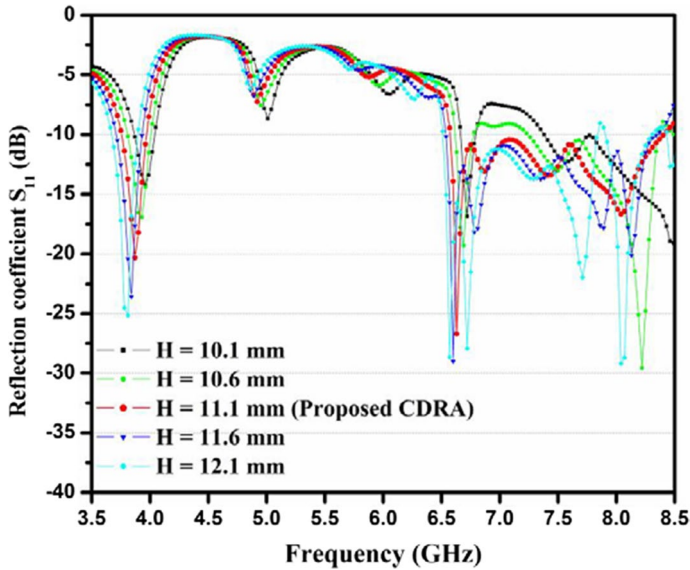


Fig. 5 Reflection coefficient versus frequency graph with the change in height (H) of CDRA

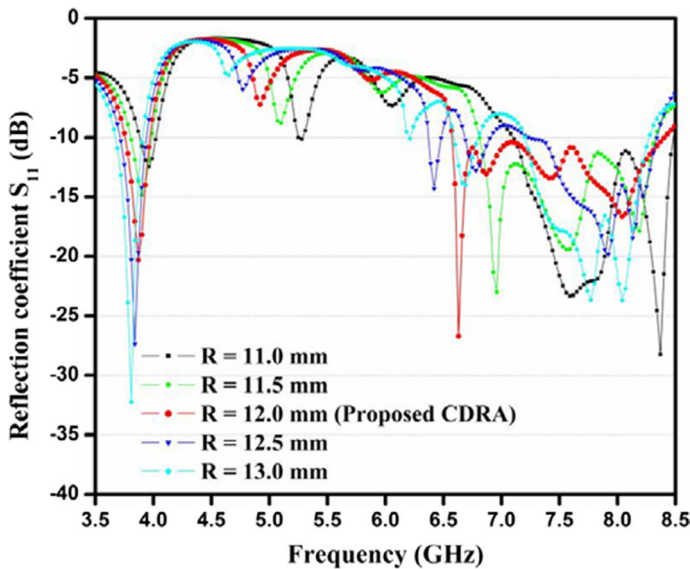


Fig. 6 Reflection coefficient versus frequency graph with the change in radius (R) of CDRA

In variation of radius (R), the three antennas are resonating in dual band with fractional bandwidth of 3.53% (140 MHz) and 17.71% (1380 MHz) for  $R = 11$  mm, 4.62% (180 MHz) and 19.96% (1510 MHz) for  $R = 11.5$  mm while 5.44% (210 MHz) and 24.29% (1820 MHz) for  $R = 12$  mm in lower and upper resonating bands respectively. The two antennas are resonating in multiband at frequencies 3.84 GHz, 6.42 GHz,

6.78 GHz and 7.92 GHz for  $R=12.5$  mm and 3.81 GHz, 6.69 GHz and 8.04 GHz for  $R=13$  mm.

In both variations, dual band of maximum fractional bandwidth 5.44% (210 MHz) between 3.75 and 3.96 GHz and 24.29% (1820 MHz) between 6.58 and 8.4 GHz is obtained for  $H=11.1$  mm and  $R=12$  mm. Thus, the optimized height ( $H$ ) and radius ( $R$ ) of CDRA are obtained 11.1 mm and 12 mm respectively.

### 3.1.3 Effect of Dielectric Constant of CDRA

The effect of dielectric constant variation on the reflection coefficient is observed for the value of dielectric constant 8.8, 9.3, 9.8, 10.3 and 10.8 as shown in Fig. 7. In variation of dielectric constant, the antenna is resonating in dual band with fractional bandwidth of 6.19% (250 MHz) and 21.62% (1680 MHz) for dielectric constant 8.8 while 6.07% (240 MHz) and 22.48% (1710 MHz) for dielectric constant 9.3. The antenna for dielectric constant 9.8, is resonating in dual band with maximum fractional bandwidth of 5.44% (210 MHz) and 24.29% (1820 MHz). The antenna for dielectric constant 10.3 is also resonating in dual band with fractional bandwidth of 6.07% (240 MHz) and 22.92% (1740 MHz) but antenna is resonating in triple band for dielectric constant 10.8 with fractional bandwidth of 5.08% (190 MHz), 6.79% (440 MHz) and 13.95% (1070 MHz).

The distribution of E-field inside the CDRA at frequency 3.87 GHz is exhibited in Fig. 8. It is confirmed from Fig. 8 that  $HEM_{11\delta}$  mode is generated, which is a basic mode [9]. This mode is generated due to the inverted pentagon slot. It is known that for the generation of  $HEM_{11\delta}$  mode, the CDRA must act like a horizontally placed magnetic dipole (inverted pentagon slots in the proposed CDRA act such magnetic dipole) [10]. This is also verified mathematically in Sect. 2.

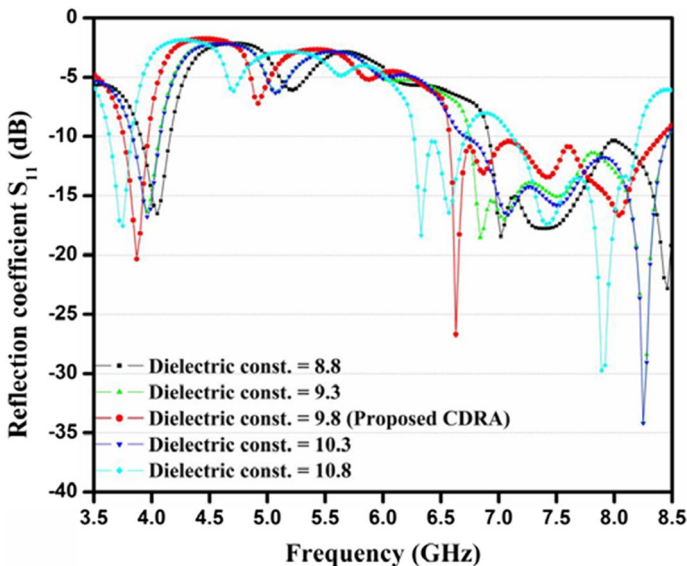
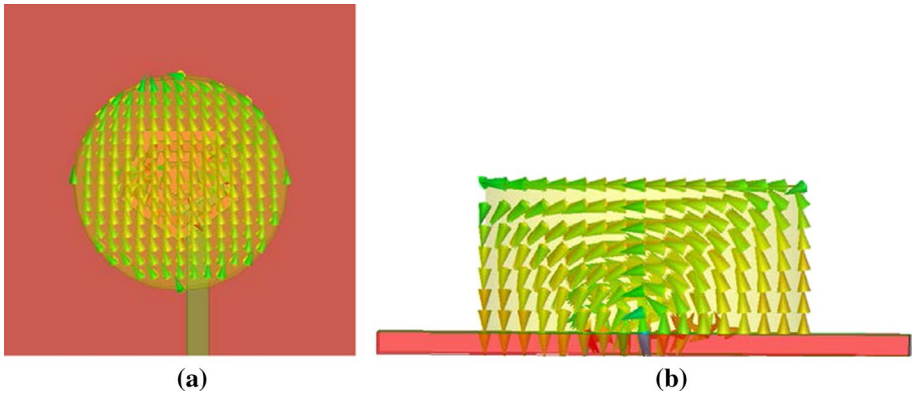


Fig. 7 Reflection coefficient versus frequency graph with the change in dielectric constant of CDRA





**Fig. 8** Distribution of E-field in CDRA at 3.87 GHz **a** top view **b** side view

### 3.2 Circular Polarization

Step to step design procedure of proposed CDRA is shown in Fig. 2 and its commensurate axial ratio graph is presented in Fig. 9. It is known that two essential conditions should be satisfied for the generation of circular polarization (CP) waves. (1) Electric field component must be orthogonally (2) Phase difference between these fields must be  $90^\circ$  [20]. It is confirmed from Fig. 9 that in step 1, step 2 and step 3, the antenna is not resonating below the 3-dB line and does not fulfill the essential condition for CP creation. But in step 4, the proposed CDRA is resonating below the 3-dB line between frequency ranges 7.52 GHz to 8.07 GHz with 7.06% (550 MHz) axial ratio BW having minimum AR value of 0.62 dB

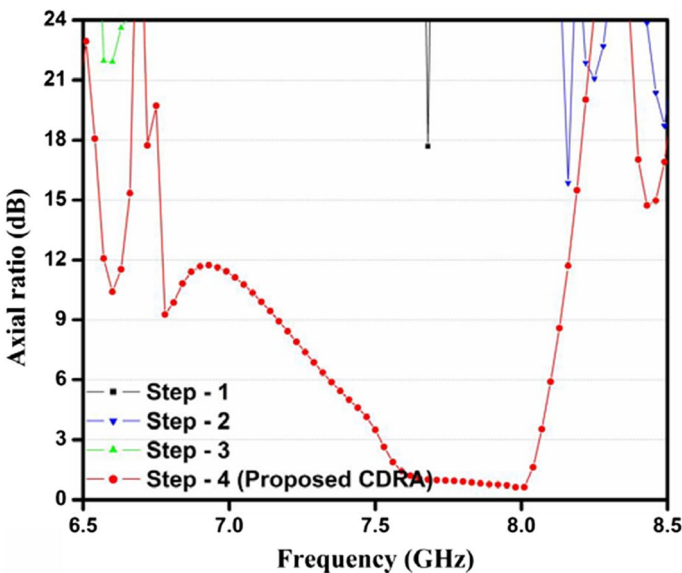


**Fig. 9** Axial ratio graph with step to step design procedure

at frequency 8.01 GHz. In the proposed radiator, the moon-like patch behaves like electric dipole whereas multiple slots of inverted pentagon shape behave like magnetic dipole that produces right angle (orthogonal) electric field [34]. However, at lower frequency, not possible to generate CP because no orthogonal component is present, that produces pure  $\text{HEM}_{118}$  mode by CDRA.

The magnitude ( $E_X/E_Y$ ) and phase difference between  $E_X$  and  $E_Y$  vs frequency graph are exhibited in Fig. 10. It can be noticed from Fig. 10, that the phase difference between  $E_X$  and  $E_Y$  is close to  $90^\circ$  and the value of magnitude ( $E_X/E_Y$ ) is near to 1 between the frequency range 7.52 GHz to 8.07 GHz. This concludes that the proposed CDRA is circularly polarized between the frequency ranges 7.52 GHz to 8.07 GHz [22].

## 4 Experimental Validation and Results Discussion

In this part, the simulated reflection coefficient of proposed CDRA is compared with experimental outcome measured by fabricated antenna. Figure 11 represents the comparative reflection coefficient graph of the experimental outcome and proposed simulated CDRA whereas Fig. 12 represents the fabricated structure of proposed CDRA. Figure 12a represents the top view with CDRA while Fig. 12b represents the feeding structure of the fabricated CDRA. Agilent Technologies' network analyzer of frequency range 300 kHz to 20 GHz is used to test the reflection coefficient of the fabricated CDRA for frequency range of 3.5 GHz to 8.5 GHz. The experimental fractional bandwidth of 8.36% (330 MHz) between 3.78 and 4.11 GHz in the lower band while the fractional bandwidth of 21.11% (1530 MHz) between 6.48 and 8.01 GHz in the upper band is obtained. However, the simulated antenna exhibits fractional bandwidth of 5.44% (210 MHz) in lower band between 3.75 and 3.96 GHz while fractional bandwidth of 24.29% (1820 MHz) in the upper band between 6.58 and 8.4 GHz. The minor changes between experimental and simulated outcome are obtained because of the effect of the

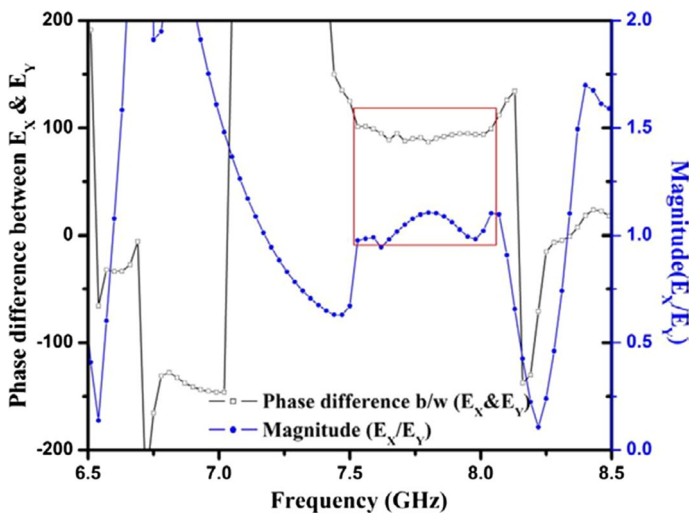


Fig. 10 Phase difference (between  $E_X$  and  $E_Y$ ) and magnitude ( $E_X/E_Y$ ) versus frequency graph of proposed CDRA

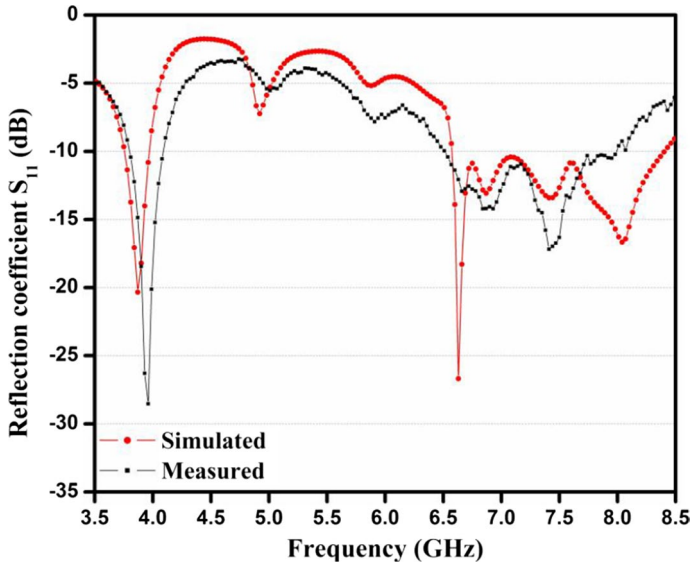


Fig. 11 Comparison of reflection coefficient graph between measured and simulated results of CDRA

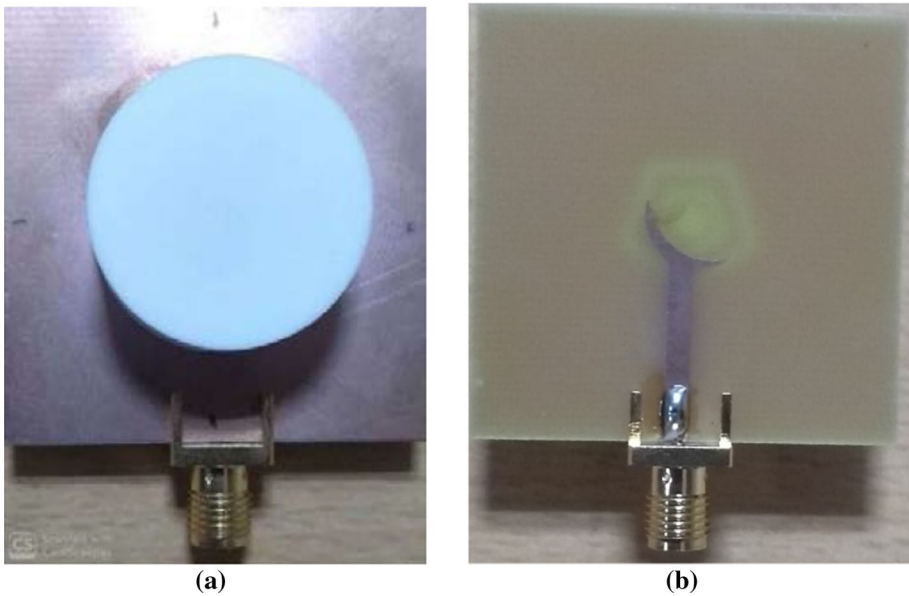
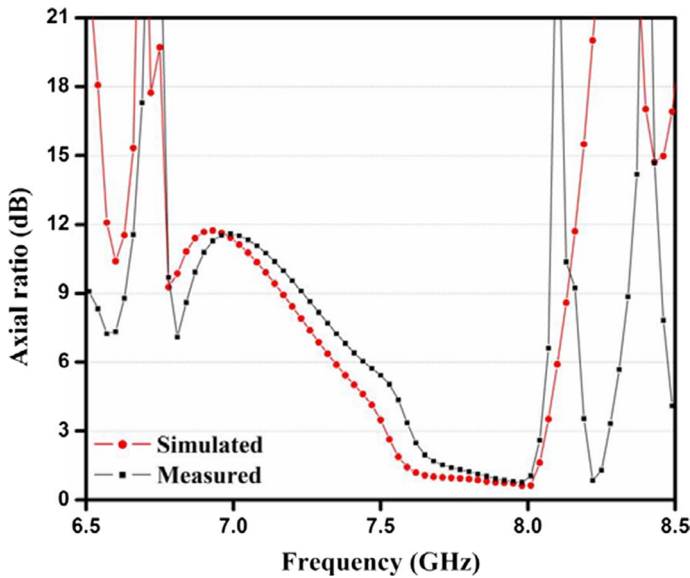


Fig. 12 Fabricated image of proposed CDRA **a** top view **b** feeding structure

thickness of connector and glue material on the substrate (to connect CDRA) [35]. In Table 2, a comparison of impedance bandwidth of proposed CDRA with the previous paper on dual-band DRA is presented. From comparison Table 2, it can conclude that the proposed CDRA has large impedance bandwidth.

**Table 2** Comparison of proposed CDRA with other dual-band DRA

References (shape of DRA)	DRA size (mm)	Excitation method	Lower freq. band (GHz)	Impedance BW (%)	Upper freq. band (GHz)	Impedance BW (%)	Gain (dB)
[24], RDRA	40×40	Aperture	3.4–3.58	5.16	5.1–5.9	14.55	5.3, 5.8
[25], CDRA	Pi×30×30	Probe feed	3.4–3.6	5.71	5.53–5.99	7.99	1.3, 3.3
[26], CDRA	Pi×30×30	Probe feed	1.87–1.92	2.64	2.92–2.66	18.03	1.4, 1
[27], RDRA	100×100	Microstrip line	1.217–1.364	11.4	1.505–1.637	8.4	5.4, 4.3
[28], CDRA	40×40	Microstrip line	2.2–2.45	10.75	3.0–3.55	16.79	3, 5.1
[31], CDRA	50×50	Microstrip line	2.36–3.22	30.82	5–5.34	6.75	7, 1
[32], CDRA	50×50	Microstrip line	2.28–2.93	24.95	4.26–4.65	8.75	6, 4.5
CDRA (Proposed)	40×40	Aperture	3.75–3.96	5.44	6.58–8.4	24.29	5.2, 6



**Fig. 13** Comparison of the axial ratio bandwidth between simulated and measured CDRA

**Table 3** Comparison of the proposed radiator with other DRA in term of axial ratio

References (Shape of DRA)	Size of DRA (mm)	Excitation method	Frequency band (GHz)	3-dB ARBW (%)
[24], RDRA	40×40	Aperture	5.18–5.34	3.4
[26], CDRA	Pi×30×30	Probe feed	2.31–2.43	5.06
[29], Semi annular DRA	35×35	Microstrip line	10.37–10.98	5.71
[30], RDRA	31×31	Microstrip line	5.15–5.36	4.57
[31], CDRA	50×50	Microstrip line	5.12–5.34	4.2
[32], CDRA	50×50	Microstrip line	4.41–4.65	5.29
CDRA (Proposed)	40×40	Aperture	7.52–8.07	7.06

The comparison between simulated and measured axial ratio vs frequency graph in broadside direction ( $\theta$  and  $\phi=0^\circ$ ) is represented in Fig. 13. The axial ratio bandwidth of proposed CDRA is measured by the dual linear pattern technique [35]. It is noticed from Fig. 13 that good similarity between measured and simulated AR graphs is obtained. Circular polarized of proposed CDRA in the frequency range 7.52 GHz to 8.07 GHz (simulated) with 3-dB axial ratio bandwidth of 7.06% (550 MHz) while 7.59 GHz to 8.05 GHz (measured) with 3-dB axial ratio BW of 5.88% (460 MHz) is obtained. Table 3 shows the comparison of 3-dB axial ratio BW of proposed CDRA and recently publishing DRA. The proposed CDRA exhibits wider axial ratio BW. It is confirmed from Table 3, that the proposed antenna is better in terms of axial ratio bandwidth (ARBW).

Figure 14a, b shows the simulated and measured radiation pattern of proposed CDRA in E and H-plane at frequency 3.87 GHz while Fig. 14c, d shows the simulated and measured LHCP and RHCP in the XZ-plane at minimum axial ratio frequency 8.01 GHz. An anechoic

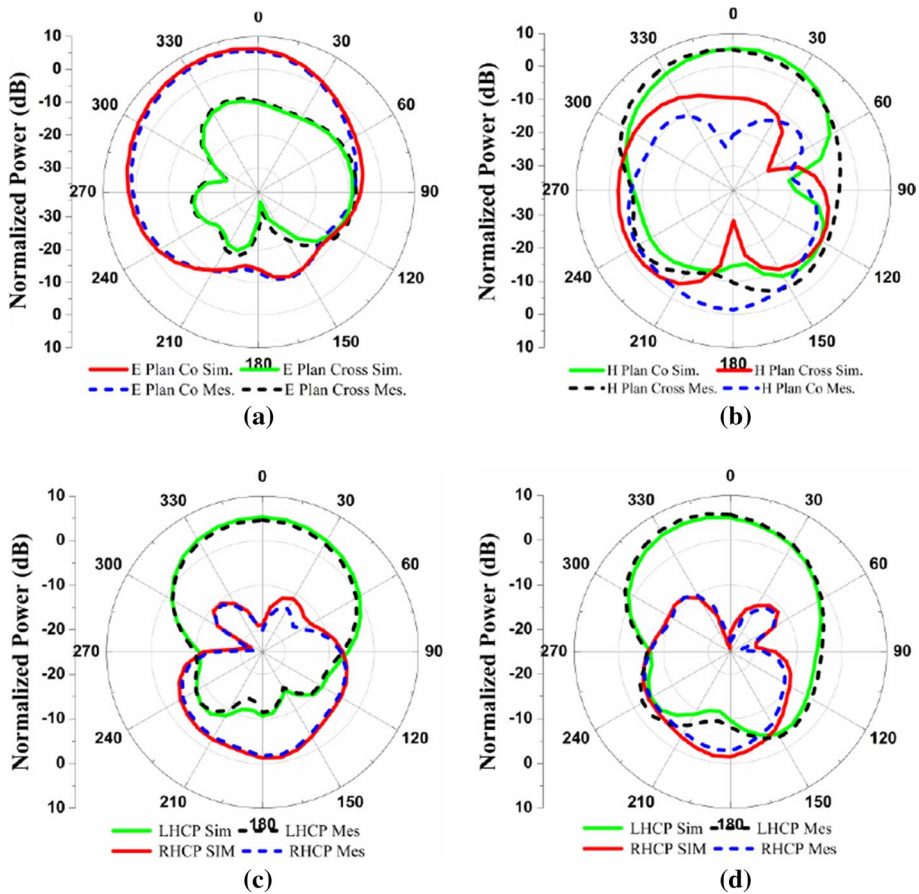


**Fig. 14** Simulated and measured radiation pattern in the XZ plane **a** E-plane at 3.87 GHz, **b** H-plane at 3.87 GHz, **c** RHCP and LHCP at 8.01 GHz ( $\theta=0^\circ$ ,  $\phi=0^\circ$ ), **d** RHCP and LHCP at 8.01 GHz ( $\theta=0^\circ$ ,  $\phi=90^\circ$ )

chamber is used for measurement purposes. A good difference has been seen between co and cross-polarization in the proposed radiator when it is kept in the principal axis that is  $\theta=0^\circ$  and  $\phi=0^\circ$ . Linear polarization characteristics ( $E_x \neq E_y$ ) are also verified by the difference between co and cross-polarization at 3.87 GHz frequency. A good agreement between measured and simulated radiation pattern is seen from radiation pattern. It is clear from Fig. 14 that the proposed CDRA exhibits LHCP pattern with an 18 dB difference between LHCP and RHCP patterns. The horizontal ( $E_H$ ) and vertical ( $E_V$ ) planes are used in the measurement of LHCP and RHCP patterns [36].

$$E_{LHCP} = \frac{1}{\sqrt{2}}(E_H - jE_V) \tag{4}$$

$$E_{RHCP} = \frac{1}{\sqrt{2}}(E_H + jE_V) \tag{5}$$

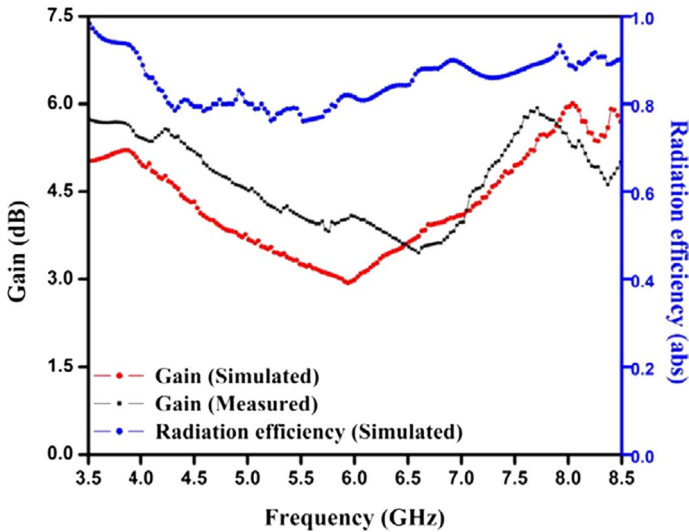


Fig. 15 Gain and radiation efficiency graph of proposed CDRA

The gain and radiation efficiency of the proposed CDRA in broadside direction ( $\theta=0^\circ$  and  $\phi=0^\circ$ ) is exhibited in Fig. 15. Two antenna methods are used to measurement of absolute gain of the proposed CDRA in the anechoic chamber [10]. In both operating band, the simulated and measured gain of proposed CDRA is more than 3 dB. The simulated radiation efficiency of proposed CDRA is more than 85% in both operating bands.

## 5 Conclusion

A dual-band dual-polarized slotted hybrid antenna has been proposed and tested experimentally. Dual-band has been achieved by the use of multiple inverted pentagon slots and CDRA. The lower operating band from 6.58 to 3.96 GHz is linearly polarized with fractional bandwidth of 5.44% (210 MHz) while the upper frequency band from 6.58 to 8.4 GHz with fractional bandwidth of 24.29% (1820 MHz) is circularly polarized from 7.52 to 8.07 GHz with 3-dB axial ratio bandwidth of 7.06% (550 MHz). A stable gain of more than 3 dB and radiation efficiency more than 85% has been obtained in both operating frequency bands. The lower frequency band from 3.75 to 3.96 GHz provides the services in S-band whereas the upper frequency band from 6.58 to 8.4 GHz comes under the category of extended C-band application and useful for the earth to space communication.

**Data Availability** Data sharing not applicable to this article as no datasets were generated or analysed during the current study.

## Declarations

**Conflict of interest** The author declares no potential conflict of interest.

## References

- Petosa, A. (2007). *Dielectric resonator antenna handbook*. Artech House.
- Chauthaiwale, P., Chaudhary, R. K., & Srivastava, K. V. (2015). Circularly polarized bowtie-shaped dielectric resonator antenna excited with asymmetric cross slot. *Microwave and Optical Technology Letters*, *57*(7), 1723–1727.
- Luk, K. M. (2003). *Dielectric resonator antenna*. Research Studies Press Ltd.
- Ding, Y., & Leung, K. W. (2009). On the dual-band DRA-slot hybrid antenna. *IEEE Transactions on Antennas and Propagation*, *57*(3), 624–630.
- Lin, Y. N., Chen, H. M., & Lin, C. H. (2009). Compact dual-band hybrid dielectric resonator antenna with radiating slot. *IEEE Antennas and Wireless Propagation Letters*, *8*, 6–9.
- Chen, H. M., Wang, Y. K., Lin, Y. F., Lin, S. C., & Pan, S. C. (2009). A compact dual-band dielectric resonator antenna using a parasitic slot. *IEEE Antennas and Wireless Propagation Letters*, *8*, 173–176.
- Guha, D., Banerjee, A., & Kumar, C. (2012). Higher order mode excitation for high-gain broadside radiation from cylindrical dielectric resonator antennas. *IEEE Transactions on Antennas and Propagation*, *60*(1), 71–77.
- Guha, D., Banerjee, A., Kumar, C., & Antar, Y. M. M. (2014). New technique to excite higher-order radiating mode in a cylindrical dielectric resonator antenna. *IEEE Antennas and Wireless Propagation Letters*, *13*, 15–18.
- Sharma, A., & Gangwar, R. K. (2016). Triple-band dual-polarized hybrid cylindrical dielectric resonator antenna with hybrid modes excitation. *Progress in Electromagnetics Research C*, *67*, 97–105.
- Sharma, A., Das, G., & Gangwar, R. K. (2017). Dual-band dual-polarized hybrid aperture-cylindrical dielectric resonator antenna for wireless applications. *The International Journal of RF and Microwave Computer-Aided Engineering*, *27*(5), 1–9.
- Kishk, A. A. (2003). An elliptic dielectric resonator antenna designed for circular polarization with single feed. *Microwave and Optical Technology Letters*, *37*(6), 454–456.
- Simeoni, M., Cicchetti, R., Yarovoy, A., & Caratelli, D. (2011). Plastic-based supershaped dielectric resonator antennas for wide-band applications. *IEEE Transactions on Antennas and Propagation*, *59*(12), 4820–4825.
- Pan, Y., & Leung, K. W. (2010). Wideband circularly polarized trapezoidal dielectric resonator antenna. *IEEE Antennas and Wireless Propagation Letters*, *9*, 588–591.
- Chaudhary, R. K., Srivastava, K. V., & Biswas, A. (2012). Wideband multilayer multi-permittivity half-split cylindrical dielectric resonator antenna. *Microwave and Optical Technology Letters*, *54*(11), 2587–2590.
- Varshney, G., Yaduvanshi, R. S., & Pandey, V. S. (2015). Gain and bandwidth controlling of dielectric slab rectangular dielectric resonator antenna. In *Annual IEEE India conference (INDICON)* (pp. 1–4).
- Huang, C. Y., Wu, J. Y., & Wong, K. L. (1999). Cross-slot-coupled microstrip antenna and dielectric resonator antenna for circular polarization. *IEEE Transactions on Antennas and Propagation*, *47*(4), 605–609.
- Huang, C. Y., & Ling, C. W. (2003). Frequency-adjustable circularly polarised dielectric resonator antenna with slotted ground plane. *Electronics Letters*, *39*(14), 1030–1031.
- Motevasselian, A., Ellgardt, A., & Jonsson, B. L. G. (2013). A circularly polarized cylindrical dielectric resonator antenna using a helical exciter. *IEEE Transactions on Antennas and Propagation*, *61*(3), 1439–2144.
- Kumar, R., & Chaudhary, R. K. (2016). A wideband circularly polarized cubic dielectric resonator antenna excited with modified microstrip feed. *IEEE Antennas and Wireless Propagation Letters*, *15*, 1285–1288.
- Kumar, R., & Chaudhary, R. K. (2017). Wideband circularly polarized dielectric resonator antenna coupled with meandered-line inductor for ISM/WLAN applications. *The International Journal of RF and Microwave Computer-Aided Engineering*, *27*(7), 1–7.
- Pathak, D., Sharma, S. K., & Kushwah, V. S. (2020). Dual-band linearly polarized integrated dielectric resonator antenna for Wi-MAX applications. *Wireless Personal Communications*, *111*, 235–243.
- Dwivedi, A. K., Sharma, A., Singh, A. K., & Singh, V. (2020). Design of dual band four port circularly polarized MIMO DRA for WLAN/WiMAX applications. *Journal of Electromagnetic Waves and Applications*, *34*(15), 1990–2009.
- Kumari, R., & Gangwar, R. K. (2017). Circularly polarized cylindrical dielectric resonator antenna excited by square ring slot with a T-shaped microstrip line. *Microwave and Optical Technology Letters*, *59*, 2507–2514.
- Gupta, A., & Gangwar, R. K. (2018). Dual-band circularly polarized aperture coupled rectangular dielectric resonator antenna for wireless applications. *IEEE Access*, *6*, 11388–11396.



25. Pan, Y. M., Zheng, S. Y., & Hu, B. J. (2014). Design of dual-band omnidirectional cylindrical dielectric resonator antenna. *IEEE Antennas and Wireless Propagation Letters*, 13, 710–713.
26. Pan, Y. M., Zheng, S. Y., & Li, W. (2014). Dual-band and dual-sense omnidirectional circularly polarized antenna. *IEEE Antennas and Wireless Propagation Letters*, 13, 706–709.
27. Wang, X. C., Sun, L., Lu, X. L., Liang, S., & Lu, W. Z. (2017). Single-feed dual-band circularly polarized dielectric resonator antenna for CNSS applications. *IEEE Transactions on Antennas and Propagation*, 65(8), 4283–4287.
28. Sharma, A., Tripathi, D. K., Das, G., & Gangwar, R. K. (2019). Novel asymmetrical Swastik-shaped aperture coupled cylindrical dielectric resonator antenna with dual-band and dual-sense circular polarization characteristics. *Microwave and Optical Technology Letters*, 61(2), 405–411.
29. Lee, J. M., Kim, S. J., Song, C. M., Yang, Y., Lee, K. Y., & Hwang, K. C. (2015). Circularly polarized semi-eccentric annular dielectric resonator antenna for X-band applications. *IEEE Antennas and Wireless Propagation Letters*, 14, 1810–1813.
30. Khalily, M., Kamarudin, M. R., Mokayef, M., & Jamaluddin, M. H. (2014). Omnidirectional circularly polarized dielectric resonator antenna for 5.2-GHz WLAN applications. *IEEE Antennas and Wireless Propagation Letters*, 13, 443–446.
31. Sharma, A., Das, G., & Gangwar, R. K. (2017). Dual-band circularly polarized hybrid antenna for WLAN/WiMAX applications. *Microwave and Optical Technology Letters*, 59(10), 2450–2457.
32. Sharma, A., Ranjan, P., & Sikandar, S. (2020). Dual band ring shaped dielectric resonator based radiator with left and right handed sense circularly polarized features. *IETE Technical Review*, 38, 1–9.
33. Chahat, N., et al. (2019). Advanced cubesat antennas for deep space and earth science missions: A review. *IEEE Antennas and Propagation Magazine*, 61, 37–46.
34. Kraus, J. D. (2003). *Antennas for all applications*. McGraw-Hill.
35. Stutzman, W. L., & Thiele, G. A. (1981). *Antenna theory and design* (Vol. 23). Wiley.
36. Toh, B. Y., Cahill, R., & Fusco, V. F. (2003). Understanding and measuring circular polarization. *IEEE Transactions on Education*, 46(3), 313–318.

**Publisher's Note** Springer Nature remains neutral with regard to jurisdictional claims in published maps and institutional affiliations.



**Chandravilash Rai** is currently working as a Research scholar in the Department of Electronics and Communication Engineering, Indian Institute of Information Technology Allahabad, Prayagraj, U.P. (India). In 2009 he received his B.Tech. Degree in Electronics and Communication Engineering from the UPTU, Lucknow, and Completed M.Tech in digital communication Engineering from Rajiv Gandhi Proudyogiki Vishwavidyalaya, University in Bhopal, Madhya Pradesh India, in 2017. His research interests include RF & Microwave, Dielectric resonator antenna, Microstrip patch antennas, Wireless communication and Antenna theory.



**Amit Singh** is currently pursuing a Ph.D. from IIIT Allahabad, Uttar Pradesh India. He had completed M.Tech. in the year 2010 from IIT (BHU), Varanasi. He had completed B.Tech. in the year 2006 from Uma Nath Singh Institute of Engineering and Technology (V.B.S. Purvanchal University) Jaunpur, Uttar Pradesh in Electronics and Communication Engineering. He is an expert in the VLSI fabrication and antenna domain. Presently he is working on VLSI fabrication and simulation on Metal/Ferroelectric/Insulator/Silicon structure for non-volatile memory applications.



**Dr. Sanjai Singh** received his Ph.D. degree from the University of Allahabad, India. Currently, he is an Associate Professor at the Electronics and Communication Engineering Department at the Indian Institute of Information Technology, Allahabad, India. His research interests Modern Physics, Semiconductor Devices, Wave Theory, antenna theory.



**Dr. Ashutosh Kumar Singh** received his M. Tech. degree from MNNIT Allahabad and a Doctoral degree from the Indian Institute of Information Technology, Allahabad, India. Currently, he is an Assistant Professor at the Electronics and Communication Engineering Department at the Indian Institute of Information Technology, Allahabad, India. His research interests include control systems, electronic circuits, networked control systems, and practical applications of control system theory, antenna theory.



**Ramesh Kumar Verma** is born on 15, June 1985 in Ambedkar Nagar, Uttar Pradesh India. He is currently pursuing a Ph.D. from AKTU Lucknow, Uttar Pradesh India. He had completed M.Tech. in the year 2015 from Bundelkhand Institute of Engineering and Technology Jhansi, in Digital communication. He had completed B.Tech. in the year 2009 from Raj Kumar Goel Institute of Technology Ghaziabad in Electronics and Communication Engineering. He is an expert in antenna designing, fabrication, IE3D simulation software and Particle Swarm Optimization (PSO) Algorithm. Presently he is working on optimization of microstrip patch antenna with PSO and curve fitting.